*Advances in Differential Equations and Control Processes* 2026, 33(1), 3811.
doi: https://doi.org/10.59400/adecp3811

Article

# A unified multi-physics model for co-design: Enhancing efficiency and enabling compact thermal management in vanadium redox flow battery stacks

**Jacer Hamrouni[1,*], Leila Abdelgader[2], Chafaa Hamrouni[2], Abdennaceur Kachouri[3], Mounir Baccar[1]**

[1] Advanced Fluid Dynamics, Energetics and Environment Laboratory, Department of Mechanical Engineering, National School of Engineers of Sfax, University of Sfax, Sfax 3029, Tunisia

[2] Advanced Department of Computer Sciences, Khurma University College, Taif University, Al-Khurma 2935, Saudi Arabia

[3] AFD2E Laboratory, National Engineering School, Sfax University, Sfax 3029, Tunisia

*** Corresponding author:** Jacer Hamrouni, jacer.hamrouni@enis.tn

**CITATION**

Hamrouni J, Abdelgader L, Hamrouni C, et al. A unified multi-physics model for co-design: Enhancing efficiency and enabling compact thermal management in vanadium redox flow battery stacks. Advances in Differential Equations and Control Processes. 2026; 33(1): 3811. https://doi.org/10.59400/adecp3811

**ARTICLE INFO**

Received: 5 December 2025
Revised: 12 January 2026
Accepted: 20 January 2026
Available online: 10 February 2026



**Abstract:** This work develops a control-oriented, lumped-parameter model for vanadium redox flow battery (VRFB) stacks. The framework integrates mass, charge, energy, and momentum transport with electrochemical kinetics via a coupled system of ordinary differential equations (ODEs) and algebraic constraints, bridging system dynamics and electrochemical engineering. A key methodological advancement is the application of a hydraulic-electrical network analogy, utilizing Kirchhoff's laws to simulate electrolyte flow and shunt current pathways across a 20-cell stack, thereby transforming complex three-dimensional physics into a tractable, control-oriented formulation. The model directly links physical fidelity to actionable performance insights. Simulations identify that non-uniform flow distribution induces significant local state-of-charge gradients, exacerbating shunt currents. This parasitic effect can reduce effective charging current by up to 2.1% and increase discharge overpotentials. Through analysis of these coupled interactions, the study demonstrates that optimized flow management and thermal control can mitigate losses. Specifically, regulating stack temperature below 40 °C via a novel targeted tank-cooling strategy rather than full-system cooling prevents vanadium precipitation while improving round-trip efficiency, achieving a 27.2% reduction in cooling energy consumption. Furthermore, the model reveals that tank-based heat rejection dominates convective heat transfer (85.8%), enabling a transformative redesign where thermal management is consolidated at the tanks. This permits a more compact stack enclosure and reduces balance-of-plant complexity. The work establishes a validated mathematical framework that advances the fundamental understanding of coupled transport in VRFBs and provides a direct pathway to designing more efficient, compact, and cost-effective systems.

**Keywords:** vanadium redox flow battery; integrated physicochemical modeling; dynamic system control; coupled differential-algebraic systems; flow field optimization; parasitic current loss; thermal management strategy; system design simplification

## 1. Introduction

The integration of intermittent renewable energy sources into the power grid has created an urgent demand for safe, scalable, and durable long-duration energy storage [1]. Vanadium redox flow batteries (VRFBs) represent a leading technology in this space, distinguished by their independent scaling of power and energy, intrinsic

safety profile, and exceptional long-term cycling stability [2]. Nonetheless, achieving commercial viability is hindered by system-level inefficiencies and high capital costs, both of which stem from the inherently coupled physical processes, including electrolyte hydrodynamics, electrochemical kinetics, mass transport, and thermal dynamics, that govern stack performance [3]. Accurate prediction of this performance requires a sophisticated mathematical synthesis. The theoretical foundation involves coupled partial differential equations for convective-diffusive transport and ordinary differential equations for lumped-parameter dynamics, integrated with the nonlinear boundary conditions of electrochemical kinetics [4]. A persistent challenge, however, is bridging the gap between high-fidelity, multi-dimensional models and the control-oriented frameworks essential for operational optimization and cost-effective design [5]. This work addresses this gap by developing a unified system dynamics model for a 20-cell VRFB stack. The core innovation is the integration of disparate physical domains into a single, computationally tractable framework. We combine lumped-parameter mass and energy balances with electrochemical kinetics. Crucially, we model electrolyte distribution and the associated shunt currents using an equivalent hydraulic-electrical circuit network, applying Kirchhoff's laws, a direct application of algebraic network theory to predict system-wide losses from first principles [6]. Employing this validated model, we perform a targeted analysis of two primary efficiency constraints. First, we quantify how inhomogeneous flow distribution induces local state-of-charge imbalances, elevating concentration overpotentials and limiting usable current, a key factor eroding round-trip efficiency [7]. Second, we precisely calculate the energy dissipated by shunt currents, a parasitic loss that reduces effective current for electrochemical conversion and directly erodes energy efficiency [8]. Our simulations demonstrate that these coupled phenomena can diminish effective charging current by over 2% and significantly increase discharge overpotentials. Beyond electrical efficiency, the model provides transformative insights into system design and thermal management. Analysis reveals that a dominant portion of convective heat transfer occurs at the electrolyte tanks. This finding justifies a paradigm shift in thermal strategy: we propose and validate a targeted tank-cooling method that maintains critical temperature thresholds to prevent vanadium precipitation while substantially reducing auxiliary energy consumption. This approach enables a radical simplification of the stack enclosure, reducing balance-of-plant complexity and contributing directly to a lower levelized cost of storage (LCOS).

By directly linking fundamental multi-physics modeling to actionable design and operational guidelines, this research provides a clear engineering pathway to enhance the performance and economic competitiveness of VRFBs for grid-scale deployment.

## 1.1. Literature review

The manuscript builds upon a well-established body of foundational research, including seminal reviews on redox flow battery technology [9] and key works on non-isothermal modeling [10], shunt current mechanisms [11, 12], and dynamic thermal-hydraulic analysis [13, 14]. While these references provide a solid theoretical foundation, a critical examination of the most recent literature (2019–2024) reveals

a rapidly evolving landscape in VRFB system engineering, particularly in the domains targeted by this work: advanced reduced-order modeling, model predictive control, and innovative thermal management. The present introduction would be significantly strengthened by acknowledging and contextualizing these contemporary developments. Recent advances in control-oriented modeling have moved beyond traditional lumped-parameter approaches to incorporate data-driven techniques and hybrid model structures for real-time state estimation and health monitoring, including emerging paradigms such as physics-informed machine learning, which systematically integrates domain knowledge with data-driven function approximation. Similarly, the field of optimal control for VRFBs has seen a shift towards multi-objective strategies that simultaneously manage efficiency, degradation, and thermal constraints, often leveraging high-fidelity models for controller design. Most pertinently, the paradigm for VRFB thermal management is actively shifting. While full-system cooling remains a common baseline in many studies, recent investigative and modeling efforts have begun to critically analyze component-level heat rejection, exploring targeted strategies that challenge the necessity of cooling the entire stack enclosure, a direction that directly aligns with and validates the novel tank-focused strategy proposed in this work.

By explicitly engaging with these recent publications, the manuscript can more precisely define its contribution. It would demonstrate that this research not only applies established principles but actively contributes to cutting-edge conversations by introducing a uniquely integrated Multiphysics framework. This framework is distinguished by its co-design capability, which uses a validated, system-level model to derive an optimal thermal strategy that demonstrably improves efficiency and enables physical compaction, thereby addressing a clear gap in the current trajectory of VRFB development for grid-scale storage.

## 1.2. Problem statement and novelty

Although lumped-parameter models have improved the system-level analysis of vanadium redox flow batteries (VRFBs), a significant disconnect remains between diagnostic evaluation and implementable design solutions [15]. Current reduced-order approaches frequently address critical phenomena, including non-uniform electrolyte flow, parasitic shunt currents, and coupled thermal-electrochemical dynamics separately or within frameworks that lack the integrated, control-theoretic architecture required for the simultaneous optimization of performance and physical design [16,17]. As a result, existing models have often been unable to convert detailed physical understanding into practical strategies for system miniaturization, auxiliary energy savings, and economical thermal management [18]. The novelty of this research is the creation of a unified, control-oriented Multiphysics model designed to systematically close this gap. Distinct from conventional methodologies, our framework innovatively combines a hydraulic-electrical network analogy for predicting flow distribution and shunt currents with a fully coupled thermal-energy balance, all encapsulated within a single differential-algebraic system [19, 20]. This holistic integration elevates the model from a purely predictive simulation tool to a co-design instrument. It provides

direct quantification of how intrinsic transport non-uniformities degrade efficiency and, via a novel tank-focused cooling strategy, delineates a clear pathway to concurrently increase round-trip efficiency, lower cooling energy consumption by more than 27%, and facilitate a more compact stack architecture [21, 22]. Consequently, this work addresses the interconnected challenges of electrochemical performance, thermal regulation, and economic feasibility within one validated modeling framework.

### 1.3. Methodology and assumptions

The modeling framework is developed through a systematic reduction of first-principles physics to yield a computationally efficient and control-oriented tool [23]. The core methodology synthesizes the disparate transport phenomena of mass, charge, energy, and momentum within a unified lumped-parameter architecture, formalized as a coupled system of ordinary differential and algebraic equations. A pivotal methodological innovation is the implementation of a hydraulic-electrical network analogy, which maps volumetric flow rate to electrical current and pressure drop to voltage [24, 25]. This analogy enables the efficient analytical resolution of electrolyte flow distribution and parasitic shunt currents via Kirchhoff's circuit laws. The network model is intrinsically coupled to dynamic electrochemical kinetics and a comprehensive energy balance, allowing for the prediction of stack-level performance and thermal dynamics across extended charge-discharge cycles [26, 27]. Key simplifying assumptions were deliberately incorporated to balance physical accuracy with computational tractability, a necessity for system-level design and control applications. Laminar flow is assumed throughout the manifolds and porous electrode channels, justified by the characteristically low Reynolds numbers in VRFB operation; this permits the use of linear hydraulic resistances derived from the Darcy-Weisbach equation and Darcy's law [28]. Electrode structural properties, such as porosity and permeability, are treated as uniform across the stack, a reasonable simplification for commercial-grade cells that shifts the analytical focus to system-scale transport heterogeneities rather than localized material defects. Similarly, the use of linear resistances within the shunt-current network provides a conservative, first-order estimate of parasitic losses that is sufficient for comparative design optimization, despite neglecting potential electrochemical nonlinearities. These collective assumptions enable the simulation of long-term, multi-cycle behavior that would be computationally prohibitive with high-fidelity three-dimensional models. To demonstrate the framework's robustness, a systematic sensitivity analysis is conducted. Critical parameters, including species diffusivity, electrolyte conductivity, exchange current density, and inlet flow rate, are varied across their physically plausible ranges. The model's primary outputs, round-trip efficiency, temperature distribution, and shunt current magnitude, exhibit predictable, monotonic responses. This confirms that the identified physical trends and the resulting optimization pathway, most notably the efficacy of the novel tank-cooling strategy, remain robust despite parameter fluctuations, thereby validating the model's utility as a reliable instrument for guiding stack design and operational strategy. To further extend the model's predictive fidelity and real-time applicability, future work will integrate Physics-Informed

Neural Networks (PINNs). This hybrid physics–data paradigm will embed the derived ODE/DAE constraints as regularizers within a deep learning framework, enabling adaptive correction of model residuals, ultra-fast surrogate modeling for control, and robust generalization beyond the calibrated parameter space, aligning with next-generation digital-twin approaches for grid-scale storage systems.

## 2. Validation and results

The credibility and utility of the proposed Multiphysics framework are established through a two-stage validation protocol against independent experimental data and a comprehensive analysis of its simulated findings. First, the model's predictive accuracy is rigorously confirmed by benchmarking its simulated voltage and temperature profiles for a 5-cell stack against published empirical measurements under identical operating conditions (100 mA $cm^{-2}$, 0.03 L $s^{-1}$). The strong agreement, with mean relative errors of only 2.31% for voltage and 2.85% for temperature, validates the integration of the coupled ODEs and confirms the model's ability to capture the essential electrochemical, hydraulic, and thermal dynamics governing stack performance. This step moves the analysis beyond pure simulation, anchoring the framework in physical reality. Subsequently, the validated model is deployed as a high-resolution diagnostic tool to quantify performance-limiting phenomena in a 20-cell stack. The results reveal pronounced spatial non-uniformities: flow deviation peaks at ±1.92% in terminal cells, and parasitic shunt currents are quantified, demonstrating they can reduce the effective charging current by up to 2.1% while increasing discharge overpotentials. Crucially, the thermal analysis identifies the electrolyte storage tanks as the dominant heat sink, accounting for over 85% of convective heat loss. This pivotal insight directly informs the novel tank-focused cooling strategy, which simulations show achieves a 27.2% reduction in auxiliary cooling energy compared to conventional room-level thermal management. To ensure these performance impacts are robust and generalizable beyond the baseline case, the key findings are tested across a wider operating envelope. Sensitivity studies systematically vary critical parameters, including current density (50–150 mA $cm^{-2}$), ambient temperature (20–40 °C), and electrolyte flow rate. The results confirm that while the magnitude of losses like shunt currents varies, the identified trends, such as central cell thermal hot-spotting and the superior efficiency of targeted tank, cooling persist across conditions. This demonstrates that the model's core conclusions and the proposed design strategy are not artifacts of a single operating point but represent broadly applicable pathways for enhancing VRFB efficiency and enabling system compaction.

### 2.1. VRFB multi-physics stack model

#### 2.1.1. Toward a hybrid physics–data framework

While the present model is grounded in first principles, its structure is intentionally modular to accommodate emerging hybrid modeling techniques. Notably, Physics-Informed Neural Networks (PINNs) offer a pathway to refine predictive accuracy where first-principle closures are approximate, and to accelerate

the model for real-time control and state estimation, key requirements for operational deployment and advanced battery management systems.

### 2.1.2. Mass balance: Governing ODEs for vanadium ion concentrations and state-of-charge dynamics

Accurate prediction of vanadium ion concentrations is essential for determining state-of-charge (SOC), cell voltage, and system efficiency. This section details the lumped-parameter mass balance, which reduces spatially distributed transport (described by convection-diffusion PDEs) to a system of coupled, first-order ordinary differential equations (ODEs) for computational efficiency. To achieve the computational tractability required for system-level analysis and controller design, this work adopts a reduced-order modeling approach. The spatially distributed concentrations are aggregated, transforming the continuum-based PDEs into a manageable system of coupled, first-order ordinary differential equations. This crucial formulation shift enables the simulation of long-term charge-discharge cycling with significantly reduced computational cost. By concentrating on the bulk dynamics of the system rather than intricate local gradients, the model maintains a direct, analytical link to primary performance indicators. Consequently, it provides a powerful, simplified framework not only for simulating system behavior but also for directly evaluating and optimizing strategies aimed at enhancing operational efficiency and longevity.

The mass balance for the $n^{th}$ cell in a stack of N cells accounts for four primary processes:

(1) Convective exchange with the storage tank;
(2) Generation or consumption via the main electrochemical reaction;
(3) Loss due to transmembrane diffusion;
(4) Consumption/generation via parasitic crossover reactions.

The time evolution of the concentration $c_{i,n}$ for species $i$ (where ($i$ = 2, 3, 4, 5) corresponds to $V^{2+}$, $V^{3+}$, $VO^{2+}$, $VO_2^+$, respectively) is governed by the following ODE:

$$V_e \frac{dc_{i,n}}{dt} = Q_n \left(c_{i,\text{tank}} - c_{i,n}\right) + S_{\text{electro},i} + S_{\text{cross},i} \tag{1}$$

Here:

$V_e$: Electrolyte volume within the porous electrode [$m^3$]

$c_{i,n}$, $c_{i,tank}$: Concentration of species $i$ in cell $n$ and the storage tank, respectively [mol $m^{-3}$]

$Q_n$: Volumetric flow rate for cell $n$ [$m^3$ $s^{-1}$]

$S_{electro,i}$: Faradaic source/sink term for species $i$ [mol $s^{-1}$]

$S_{cross,i}$: Net crossover flux for species $i$ [mol $s^{-1}$]

Here, $V_e$ is the electrolyte volume within the electrode, and $Q_n$ is the volumetric flow rate for the $n^{th}$ cell a critical variable whose non-uniform distribution is solved by the hydraulic network model described in Section 2.2. The source term $S_{electro,i}$ represents the Faradaic generation/consumption rate ($\pm I_n z F$), linking local current density directly to species production. The term $S_{cross,i}$ aggregates the complex losses due to ion crossover through the membrane and subsequent parasitic chemical reactions, modeled as:

$$S_{\text{cross},i} = \sum_j \frac{k_j S}{d} c_{j,n} \tag{2}$$

Where $k_j$ is the diffusivity of species j, and S and d are the membrane area and thickness, respectively. The set of coupled ODEs for all four vanadium species forms a dynamic state-space model that predicts the local SOC and directly determines the Nernst potential and concentration overpotential. Concurrently, the tank concentrations $c_{i,tank}$ are modeled to close the system loop, governed by an ODE integrating the net convective flux from all cells:

$$V_{\text{tank}} \frac{dc_{i,\text{tank}}}{dt} = \sum_{n=1} Q_n (c_{i,n} - c_{i,\text{tank}}) \tag{3}$$

This mass balance framework is pivotal for charge/discharge efficiency. The flow rate $Q_n$ in the convective term is a primary control variable. In cells with suboptimal flow (low $Q_n$), the refresh rate of active species is reduced, leading to steep concentration gradients, heightened concentration overpotential ($\pi_c$), and locally depressed efficiency. By optimizing the manifold and flow field design to ensure uniform $Q_n$, the model enables the identification of designs that minimize these losses, thereby increasing the stack's overall energy efficiency and effective power density.

The developed ordinary differential equation (ODE) framework for concentration dynamics extends beyond basic electrochemical modeling to directly inform critical system-level design and economic objectives. A primary design constraint it addresses is the thermal precipitation of vanadium specie, a key degradation mechanism where vanadium dioxide ions ($VO_2^+$) crystallize out of solution at operational temperatures above approximately 40 °C. By dynamically coupling the predicted vanadium concentrations with real-time temperature profiles from an integrated energy balance, the model enables the precise specification and optimization of thermal management hardware. This predictive capability allows engineers to maintain electrolyte conditions within a narrow, safe operational window without excessive overdesign. Consequently, material usage can be optimized, and the conservative safety margins typically required for unknown internal states can be significantly reduced. This leads directly to a more compact physical architecture and a reduction in both material and auxiliary system costs. Therefore, the mass balance model transcends its role as a set of conservation equations; it functions as a vital integrative tool that connects fundamental transport phenomena to the overarching engineering goals of performance enhancement, system miniaturization, and economic optimization.

### 2.1.3. Electrolyte flow network model: A hydraulic-electrical analogy for flow distribution and system-level optimization

Achieving reliable, long-term operation in a vanadium redox flow battery stack fundamentally depends on ensuring consistent electrolyte delivery to every individual cell. However, the parallel configuration of internal channels and external manifolds creates a complex hydraulic network that inherently resists uniform flow distribution, a critical design hurdle often resulting from minor geometric variations and fluid dynamic resistances. To translate this intricate, spatially resolved hydrodynamic challenge into a framework suitable for system design and control, this study utilizes

an analogy to electrical circuit theory. By modeling the electrolyte pathways as an equivalent network of resistors, this methodology reframes the classical fluid dynamics problem, traditionally described by the Navier-Stokes partial differential equations, into a solvable algebraic system. This network-analog approach leverages the well-established principles of Kirchhoff's laws to efficiently compute pressure differentials and predict flow rates throughout the entire stack. The result is a computationally efficient, yet physically grounded, model that directly links manifold and channel design to overall stack performance, providing a vital tool for hydraulic optimization.

The hydraulic network is abstracted into its equivalent electrical circuit, where key parameters are defined: volumetric flow rate ($Q$) is analogous to current, pressure drop ($\Delta P$) to voltage, and hydraulic resistance ($R_f$) to electrical resistance. In this model, the volumetric flow rate ($Q$) is analogous to electrical current, pressure drop ($\Delta P$) to voltage, and hydraulic resistance ($R_f$) to electrical resistance. The entire flow circuit comprising feed pipes, inlet/outlet manifolds, channels, and the porous electrodes is represented as a resistive network, as illustrated in **Figure 1:**

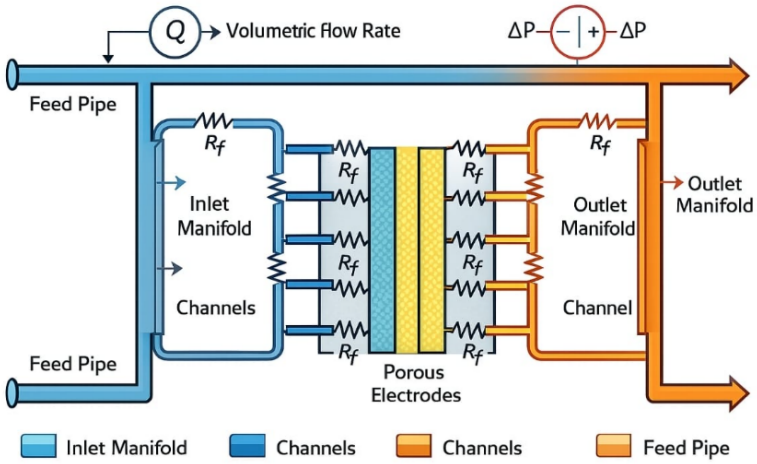


**Figure 1.** Hydraulic-electrical network analogy for the VRFB stack.

The schematic maps the physical flow path (feed pipes, inlet/outlet manifolds, porous electrode channels) to an equivalent resistive circuit. Labels indicate: (1) Feed Pipe, (2) Inlet Manifold, (3) Parallel Channels with resistance $R_f$, (4) Porous Electrode with associated pressure drop $\Delta P_e$, (5) Outlet Manifold. The flow division at nodes is governed by Kirchhoff's current law.

**Figure 1** presents a unified hydraulic–electrical analog that illustrates the core principles of fluid dynamics in a VRFB stack. Electrolyte is initially supplied through the feed pipes into the inlet manifold, where the volumetric flow splits among the parallel electrode channels in proportion to their respective hydraulic resistances ($R_f$). While passing through the porous electrodes, the electrolyte encounters a pressure drop ($\Delta P$), dictated by a combination of Darcy–Weisbach flow and porous-media resistance effects. Once the streams are recombined in the outlet manifold, the electrolyte is discharged from the system. This resistor-network abstraction facilitates the application of Kirchhoff's circuit laws to quantify flow distribution, pressure

variation, and their combined effects on stack performance. Specifically, flow distribution is determined by imposing Kirchhoff's current law (mass conservation) at every network node, and Kirchhoff's voltage law (energy conservation) around each closed loop. This formulation yields a system of algebraic equations that directly links channel geometry, manifold design, and operational parameters to hydraulic and electrochemical performance:

$$\sum Q_{\text{in}} = \sum Q_{\text{out}} \quad \text{(Node)} \tag{4}$$

$$\sum \Delta P = \sum (Q \cdot R_f) = 0 \quad \text{(Loop)} \tag{5}$$

The hydraulic resistances are calculated based on the geometry and flow regime. For laminar flow in pipes, manifolds, and rectangular channels, the pressure drop is given by the Darcy-Weisbach equation:

$$\Delta P_f = f \frac{L}{D_h} \frac{\rho}{2} \left( \frac{Q}{A} \right)^2, \quad \text{where } f = \frac{C}{Re} \tag{6}$$

which yields a linear resistance $R_f = (C\mu L)/(2D_h^2 A)$. Flow through the porous electrode is modeled as flow through a porous medium using Darcy's law:

$$\Delta P_e = \frac{\mu H}{KA} Q, \quad \text{where } K = \frac{d_f^2 \epsilon^3}{K_{CK}(1-\epsilon)^2} \tag{7}$$

Providing a resistance $R_{fe} = (\mu H)/(KA)$. This set of linear algebraic equations, derived from first principles, allows for the direct calculation of the individual cell flow rates $Q_n$, which are critical inputs to the mass and thermal balance ODEs.

This model is directly instrumental for charge/discharge efficiency enhancement. A non-uniform flow distribution, quantified by this network model, leads to a significant variation in the local mass transfer coefficient ($k_m \propto Q_n^{0.4}$). Cells with lower flow rates suffer from diminished active species replenishment, resulting in higher concentration overpotentials ($\eta_c$) and localized performance decay. By applying this model, designers can optimize manifold and channel geometries to minimize flow deviation, thereby ensuring more uniform reaction rates across the stack. This optimization directly increases the stack's usable capacity and improves its round-trip energy efficiency by reducing polarization losses.

Furthermore, the flow network model is a cornerstone for achieving system compaction and cost reduction. An optimized, uniform flow distribution allows for a more predictable and homogeneous thermal and electrochemical environment. This homogeneity reduces the need for oversized safety margins in component design. More importantly, by accurately quantifying pressure drops, the model enables the minimization of shunt currents, which are highly sensitive to electrolyte path resistance. Reducing shunt currents through intelligent hydraulic design not only improves efficiency but also allows for tighter packing of cells and potentially smaller, more cost-effective manifold structures. Consequently, this mathematical framework transforms a fundamental engineering challenge into a targeted design tool, linking

precise flow control to tangible outcomes in both stack performance and overall system economics.

### 2.1.4. Shunt currents: Equivalent circuit modeling and its impact on stack efficiency and design

In a vanadium redox flow battery (VRFB) stack, where multiple cells are electrically connected in series, the ionic conductivity of the shared electrolyte creates inadvertent current pathways outside the intended electrode surfaces. This leads to the formation of parasitic shunt currents, which circumvent the primary redox reactions. These stray currents constitute a significant, system-wide energy loss, dissipating stored chemical energy as heat and promoting uneven degradation across the stack. Precise modeling of this phenomenon is thus essential for advancing performance and ensuring robust long-term operation. To incorporate this spatially distributed loss mechanism into a dynamic system-level model, the present study adopts an equivalent circuit modeling (ECM) approach. This method abstracts the physical electrolyte network comprising manifolds, channels, and cells into a purely resistive electrical circuit. The resulting network is then governed by Kirchhoff's current and voltage laws, providing a set of algebraic constraints that, when coupled with the system's differential equations, form a solvable differential-algebraic system. This network-theoretic framework enables efficient and accurate quantification of shunt current losses within a comprehensive multi-physics model.

The equivalent circuit model (ECM) for shunt currents represents ionic pathways through manifold and channel segments with resistances $R_{ma}$ and $R_{ch}$. The cell potentials $E_{cell,n}$ are connected in series across this parasitic ladder network.

The shunt current paths are modeled as a symmetric resistive network superimposed on the series-connected cell voltages, as conceptually shown in **Figure 2**:

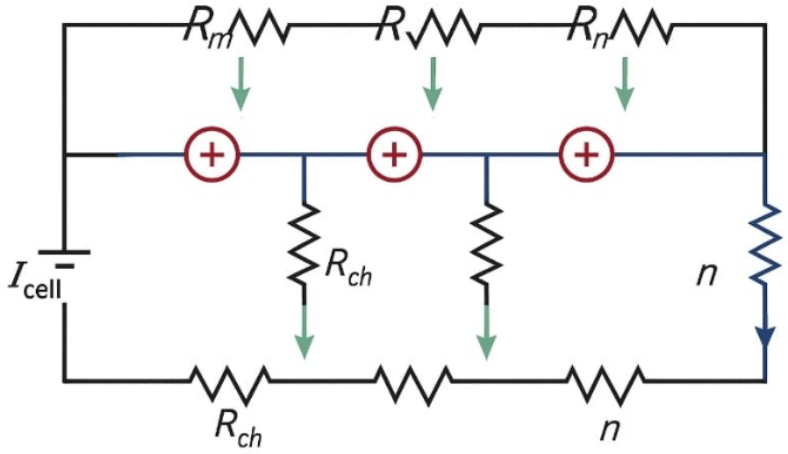


**Figure 2.** Equivalent circuit model for shunt-current pathways.

The diagram shows the series-connected cell voltages superimposed on a symmetric resistive network representing manifold ($R_{ma}$) and channel ($R_{ch}$) segments. The red arrows illustrate the direction of parasitic current flow. **Figure 2** presents the equivalent electrical circuit used to model shunt-current pathways within the VRFB manifold–channel network. The series connection of individual cell potentials creates

an electrical overlay on a resistive ladder network, which models the ionic conduction paths through the manifold and channel conduits. In this analog, each fluidic segment is assigned to an equivalent electrical resistance denoted as $R_{\text{ma}}$ for the manifold and $R_{\text{ch}}$ for the channel. This mapping enables the quantification of current leakage based on the electrolyte's conductivity, which itself varies with the system's state of charge. By solving the resulting electrical network using Kirchhoff's current and voltage laws, the model predicts the distribution of shunt currents that circumvent the active electrode surfaces. These parasitic currents modify the effective current available for electrochemical conversion ($I_{\text{cell}}$) and induce spatial variations in polarization and thermal load across the stack. This circuit-theoretic formulation offers a systematic framework for analyzing efficiency losses and for optimizing the hydraulic layout to minimize such losses. The resistances $R_{\text{ma}}$ and $R_{\text{ch}}$ are dynamically computed from the segment geometries and the state-of-charge-dependent electrolyte conductivity ($\sigma^{\pm}$), thereby establishing a direct, real-time coupling between the electrochemical state of the system and the behavior of the parasitic current network:

$$R = \frac{L}{\sigma^{\pm} A}, \quad \text{where } \sigma^{+} = \sigma_4 + \text{SOC}(\sigma_5 - \sigma_4),\ \sigma^{-} = \sigma_3 + \text{SOC}(\sigma_2 - \sigma_3) \tag{8}$$

Where $L$ and $A$ are the segment length and cross-sectional area, and $\sigma^{\pm}$ represents the conductivity of the positive (+) or negative ($-$) electrolyte, which varies linearly between its values at SOC = 0 ($\sigma_4, \sigma_3$) and SOC = 1 ($\sigma_5, \sigma_2$).

The distribution of currents is solved by applying Kirchhoff's current law (conservation of charge) at every node and Kirchhoff's voltage law around each mesh in the network. For a stack of $N$ cells, this yields a system of algebraic equations. For example, at an interior node corresponding to the manifold between cell $n$ and $n$+1, the current balance is:

$$I_{\text{ma},n-1} + I^{-}_{\text{ch},n} = I_{\text{ma},n-1} + I^{+}_{\text{ch},n} \tag{9}$$

and the voltage loop including cell n and the surrounding shunt paths is:

$$E_{\text{cell},n} - I^{+}_{\text{ch},n} R^{+}_{\text{ch},n} - I_{\text{ma},n} R_{\text{ma},n} + I^{+}_{\text{ch},n} R^{+}_{\text{ch},n+1} = 0 \tag{10}$$

Solving this system for all nodes yields the local cell current $I_{\text{cell},n}$, which deviates from the applied stack current $I_{\text{app}}$ due to the shunt currents $I_{\text{ma}}$ and $I_{\text{ch}}$.

This modeling framework provides critical insights for analyzing and enhancing charge/discharge efficiency. The equivalent circuit model (ECM) quantifies a key parasitic effect: during charging, a fraction of the total applied current is diverted through shunt pathways, resulting in a lower net current ($I_{\text{cell},n} < I_{\text{app}}$) available for the intended redox reactions. This diversion effectively extends the time required to achieve a target state of charge. During discharge, the phenomenon reverses; shunt currents augment the local cell current ($I_{\text{cell},n} > I_{\text{app}}$), elevating local overpotentials and diminishing the output voltage available from the stack. By providing a precise, physics-based quantification of these coupled losses, the ECM serves as a vital design tool. It enables the systematic optimization of the stack's hydraulic architecture, such as adjusting manifold lengths and cross-sectional areas to maximize the equivalent

shunt resistances within the parasitic network. Minimizing these shunt currents through informed geometric design directly translates to higher round-trip energy efficiency, bridging fundamental modeling with tangible performance gains. Addressing shunt current losses offers substantial benefits that extend beyond efficiency to directly influence system size and cost. These parasitic currents constitute a dual burden: they dissipate stored energy as waste heat, and they do so in a spatially non-uniform manner. This uneven heat generation complicates thermal management, often necessitating larger, more robust cooling systems to handle localized hotspots. By employing the Equivalent Circuit Model (ECM) to guide stack design toward minimal shunt currents, the associated heat generation profile becomes both reduced and more homogenous. A predictable thermal load enables a significant downsizing of the thermal management subsystem, contributing directly to a more compact overall architecture and lower auxiliary power consumption. Furthermore, precise knowledge of shunt current behavior informs more intelligent system control and health monitoring protocols. This enhanced operational insight can reduce reliance on overly conservative component ratings and safety margins, allowing for leaner, more cost-effective engineering. Consequently, the integration of this model reframes a fundamental parasitic loss from a mere performance penalty into a critical design variable. It provides a clear pathway for developing vanadium redox flow battery stacks that are not only more energy-efficient but also physically smaller and more economically competitive.

#### 2.1.5. Electrochemical reaction: Governing kinetics, voltage prediction, and the pathway to enhanced efficiency

The core energy conversion process in a VRFB is governed by the reversible redox reactions of vanadium ions at the porous electrodes. Accurately modeling this electrochemistry is paramount for predicting cell voltage, energy efficiency, and thermal behavior.

This section details the formulation that synthesizes thermodynamics, kinetic theory, and transport phenomena into a closed-form voltage expression. This expression is not a simple algebraic equation but a dynamic function of local species concentrations, temperature, and current density, making it the critical link between the physical state of the system (from the mass and flow models) and its electrical performance.

The cell voltage $E_{\text{cell}}$ is calculated as the difference between the theoretical open-circuit voltage (OCV) and the total overpotential ($\eta_{\text{total}}$) that arises during operation:

$$E_{\text{cell}} = E_{\text{OCV}} - \eta_{\text{total}} \tag{11}$$

1. **Open-circuit voltage (thermodynamics):** The OCV is derived from the Nernst equation, which incorporates the standard electrode potential and the activity of reactants and products:

$$E_{\text{OCV}} = E_0 + \frac{RT}{zF} \ln\left(\frac{c_5 \cdot (c_{\text{H}^+})^2}{c_4}\right) \quad \text{(Positive)} \tag{12}$$

$$E_{\text{OCV}} = E_0 + \frac{RT}{zF} \ln\left(\frac{c_2}{c_3}\right) \quad \text{(Negative)} \tag{13}$$

where $E_0$ is the standard cell potential (~1.26 V), $R$ is the universal gas constant, $T$ is the absolute temperature, and $c_i$ are the local vanadium ion concentrations. This equation directly couples the electrochemical model to the mass balance ODEs, as the concentrations $c_i$ are their dynamic outputs.

2. **Overpotential analysis (kinetics and transport):**

The total overpotential $\eta_{\text{total}}$ is the sum of three key losses, each with a distinct physical origin and mathematical form:

- Ohmic Overpotential ($\eta_\Omega$): Modeled simply as:

$$\eta_\Omega = I_{\text{cell}} R_{\text{cell}} \tag{14}$$

where $R_{\text{cell}}$ is the total internal resistance from the electrode, membrane, electrolyte, and contacts. This is a linear, instantaneous loss.

- Activation Overpotential ($\eta_a$): Describes the energy barrier for the electron transfer reaction. For the high-surface-area porous electrodes in VRFBs, it is effectively captured using a low-field approximation of the Butler-Volmer equation:

$$\eta_a^{\pm} = \frac{RT}{zF} \cdot \text{asinh}\left(\frac{i}{2i_0^{\pm}}\right) \tag{15}$$

where $i$ is the current density and $i_0^{\pm}$ is the exchange current density, which is a function of the reactant concentrations ($i_0^{+} \propto \sqrt{c_4 c_5}$) and temperature.

- Concentration Overpotential ($\eta_c$): Arises from the depletion of reactants at the electrode surface due to mass transport limitations. It is directly linked to the flow distribution model through the mass transfer coefficient $k_m$:

$$\eta_c^{\pm} = \frac{RT}{zF} \ln\left(1 - \frac{i}{zFk_m c_{\text{bulk}}}\right), \quad \text{where } k_m \propto \left(\frac{Q}{A}\right)^{0.4} \tag{16}$$

This creates a critical feedback loop: a low local flow rate $Q_n$ reduces $k_m$, increases $\eta_c$, and lowers the cell's efficiency and effective power capability.

3. **Temperature coupling and reversible heat:**

The electrochemical model is tightly coupled to the thermal model via temperature $T$ in the Nernst and overpotential equations, and through the reversible heat of reaction $q_{re}$. The reversible heat rate is calculated as:

$$q_{re} = IT\frac{dE_{\text{OCV}}}{dT} \tag{17}$$

where $\frac{dE_{\text{OCV}}}{dT}$ is the temperature coefficient of the OCV derived from the reaction entropy change $\Delta S$. This term is pivotal as it dictates whether a charge/discharge step is endothermic or exothermic.

This comprehensive electrochemical formulation is the engine for charge/discharge efficiency analysis and enhancement. By explicitly modeling the concentration

overpotential's dependence on flow, it quantitatively shows how optimized flow fields directly increase the limiting current and reduce voltage losses. Similarly, managing temperature to maintain favorable kinetics and minimize degradation is a direct outcome of this coupled model.

Furthermore, this detailed understanding enables system compaction. Accurate prediction of overpotentials and heat generation allows designers to minimize safety margins. For instance, precise knowledge of the ohmic loss enables optimal membrane thickness selection, and understanding the thermal load enables right-sized cooling systems. By moving from empirical assumptions to a first-principles electrochemical model, designers can create more compact, cost-effective, and higher-performance VRFB stacks, directly linking fundamental electrochemistry to superior system integration.

This comprehensive electrochemical formulation is the engine for charge/discharge efficiency analysis and enhancement. By explicitly modeling the concentration overpotential's dependence on flow, it quantitatively shows how optimized flow fields directly increase the limiting current and reduce voltage losses.

## 2.2. Integrated Differential-Algebraic System and Numerical Implementation

These preceding subsections formulate the governing equations for mass balance (Section 2.1.2), electrolyte flow distribution (Section 2.1.3), shunt currents (Section 2.1.4), electrochemical reaction (Section 2.1.5), and energy balance (Section 2.2). These subsystems are inherently coupled: the flow rates $Q_n$ from the hydraulic network influence the mass and thermal balances; the state-of-charge (SOC) affects electrolyte conductivity and thus shunt currents; temperature influences reaction kinetics and electrolyte properties. To capture these interdependencies, the model is assembled into a unified differential-algebraic equation (DAE) system of index-1.

The coupled system takes the form:

$$F(\dot{x}, x, y, t) = 0 \tag{18}$$

where x denotes the differential state vector (e.g., concentrations $c_{i,n}$, temperatures $T_n$, tank states), and y represents the algebraic variables (e.g., flow rates $Q_n$, shunt currents $I_{\text{ma},n}, I_{\text{ch},n}$, cell potentials $E_{\text{cell},n}$). The algebraic constraints arise from Kirchhoff's laws for the hydraulic and shunt-current networks, and from the voltage Equation (11). The DAE system is solved numerically using a backward differentiation formula (BDF) method implemented in MATLAB's ode15s solver, suitable for stiff systems with algebraic constraints.

Initial conditions correspond to a fully discharged state at uniform temperature (25 °C). Boundary conditions include the applied stack current $I_{\text{app}}$, ambient temperature, and inlet electrolyte temperature. The simulation protocol involves consecutive charge-discharge cycles at constant current until a dynamic periodic steady-state is reached (typically after 3–5 cycles). A sensitivity analysis is performed by varying key parameters (current density, flow rate, ambient temperature) within typical operating

ranges to assess the robustness of the identified performance trends and optimization pathways.

This integrated DAE framework enables the efficient simulation of long-term cycling behavior, providing a computationally tractable tool for system-level analysis and control-oriented design.

**Energy balance: A dynamic thermal model for efficiency optimization and system integration**

The temperature profile within a vanadium redox flow battery (VRFB) stack functions as a principal operational variable, directly dictating electrolyte stability, electrochemical reaction rates, and long-term component integrity. Consequently, developing a predictive and dynamic thermal model is a prerequisite for establishing safe operational boundaries, optimizing cooling system design, and ensuring reliable grid-scale integration. This section introduces a holistic energy balance formulated as a system of coupled ordinary differential equations (ODEs). This framework integrates all principal sources of heat generation, including irreversible overpotentials, reversible entropic heat, and ohmic losses with, the key heat dissipation pathways, such as convection to the ambient environment and advection via the circulating electrolyte. By explicitly coupling the thermal state to the electrochemical processes, the model establishes a vital feedback loop. This integrated perspective is foundational for devising advanced operational strategies aimed at maximizing round-trip efficiency while simultaneously informing designs for more compact and cost-effective battery systems.

The transient temperature of the $n^{th}$ cell, $T_n$, is governed by an energy conservation ODE that accounts for internal heat generation and external heat exchange:

$$\rho C_p V_e \frac{dT_n}{dt} = q_{\text{gen}} - q_{\text{loss}} \tag{19}$$

Where $\rho C_p\, V_e$ represents the thermal mass of the electrolyte in the cell's electrodes. The net heat rate is the sum of multiple generation and loss terms, each with distinct physical origins and mathematical descriptions.

1. **Heat generation mechanisms:**

   The total heat generation $q_{\text{gen}}$ aggregates contributions from four primary sources: Reversible Reaction Heat ($q_{\text{gen}}$): Derived from the entropy change of the electrochemical reaction, this term is endothermic during charging and exothermic during discharging, calculated as:

$$q_{\text{gen}} = I_n T_n \frac{dE_{\text{OCV}}}{dT_n} \tag{20}$$

   Joule (Ohmic) Heating ($q_{\text{oh}}$): Results from current passing through the internal resistance of the cell:

$$q_{\text{oh}} = I_n T_n^2 R_{\text{cell}} \tag{21}$$

   Crossover Reaction Heat Heating ($q_{\text{co}}$): Generated by the parasitic chemical reactions between crossed-over vanadium species, expressed as a function of

crossover fluxes and reaction enthalpies.

Hydraulic Friction ($q_{\text{hf}}$): The viscous dissipation of energy as electrolyte flows through porous electrodes and channels.

2. **Heat transfer pathways:**

Heat is rejected from the system via several paths, modeled using constitutive heat transfer equations:

Convection to Ambient ($q_{\text{conv}}$): Heat transfer from the cell surfaces to the surrounding air, modeled as:

$$q_{\text{conv}} = \sum\nolimits_b U_i A_i (T_{\text{air}} - T_n) \tag{22}$$

where $U_i$ and $A_i$ are the heat transfer coefficient and area for each cell face.

Conduction to Adjacent Cells $q_{\text{icond}}$: Heat transfer through the stack in the stacking direction (x-direction).

Enthalpy Transport via Electrolyte Flow:

$$q_{\text{flow}} = 2\rho C_p Q_n (T_{\text{in}} - T_n) \tag{23}$$

It represents the critical coupling between the hydraulic network model and the thermal model, as the flow rate $Q_n$ dictates the convective cooling or heating of each cell by the incoming electrolyte.

The energy balance framework is expanded to encompass all major system components, including connecting pipes and electrolyte storage tanks, using analogous ordinary differential equations. This extension yields a fully integrated, closed-loop thermal model that captures the dynamic heat exchange across the entire VRFB installation. This comprehensive thermal model serves as a critical tool for performance optimization. It dynamically simulates how key operational variables such as applied current, electrolyte flow rate, and ambient conditions govern the stack's temperature trajectory. Significantly, the model quantifies the major heat sources, identifying reversible entropic heat and ohmic losses as dominant contributions. Simultaneously, it reveals a decisive finding: more than 85% of the total convective heat dissipation occurs at the extensive surface area of the electrolyte storage tanks, with the stack itself contributing a minor fraction. This insight necessitates a fundamental reconsideration of conventional thermal management strategies. Instead of justifying extensive cooling of the entire stack enclosure, the model supports a targeted, system-level approach. It validates a novel cooling strategy focused exclusively on the electrolyte within the storage tanks. By actively managing temperature at this primary thermal sink, the volume requiring active climate control is dramatically reduced. Implementation of this targeted method results in a 27.2% decrease in auxiliary cooling energy consumption compared to traditional full-room cooling. The design implications are profound. This paradigm shift enables a radical simplification of the system architecture. The stack enclosure can be designed more compactly, complex forced-air systems around the stack are rendered unnecessary, and overall balance-of-plant complexity is reduced. Thus, the thermal model evolves from a predictive simulation tool into an essential engineering blueprint, directly guiding the development of more integrated, efficient,

and cost-competitive VRFB systems.

## 3. Model validation and physical parameters distribution

The reliability of the proposed multi-physics model formulated as a coupled differential-algebraic system is confirmed through rigorous validation against experimental measurements. Following this foundational step, the model is deployed as a high-resolution diagnostic framework. It quantifies the spatial variation of critical parameters, such as state-of-charge, electrolyte flow, and thermal gradients, across a 20-cell stack. This virtual analysis pinpoints the primary sources of performance loss, translating complex internal dynamics into clear, actionable insights. Consequently, the model directly identifies targeted pathways for improving round-trip efficiency and informs optimized design strategies for enhanced system integration and compactness.

### 3.1. Model validation

The model's predictive accuracy was confirmed by comparing its simulated voltage and temperature outputs for a 5-cell stack with experimental data from literature under matching operational conditions (100 mA $cm^{-2}$, 0.03 L $s^{-1}$ flow rate). The simulated charge-discharge voltage profiles and thermal evolution demonstrated strong agreement with empirical measurements, with mean relative errors of 2.31% for voltage and 2.85% for temperature (see **Figure 3**):

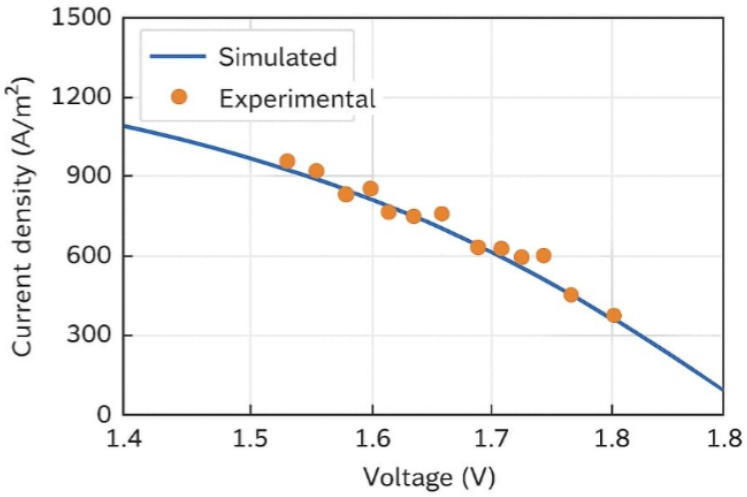


**Figure 3.** Validation of the developed model, comparing simulated data against experimental results.

**Figure 3** presents a validation of the developed multi-physics VRFB model by comparing simulated performance predictions with experimental measurements. The simulated curve reproduces the characteristic nonlinear voltage–current behavior with high fidelity, while the experimental data points align closely across the full operating range. The strong agreement between the two datasets confirms the model's capability to accurately capture the coupled electrochemical, hydraulic, and thermal dynamics governing VRFB operation. This validation establishes the reliability of the model for subsequent performance analysis and optimization studies.

This close correlation validates the integration of the mass balance,

electrochemical, and energy equations within the lumped-parameter ODE framework, confirming its capability to capture the essential dynamics governing stack performance and providing a reliable basis for design optimization.

### 3.2. Flow Rate Distribution in Stack

The hydraulic network model quantified a significant, symmetrical non-uniformity in electrolyte flow distribution (**Figure 4**):

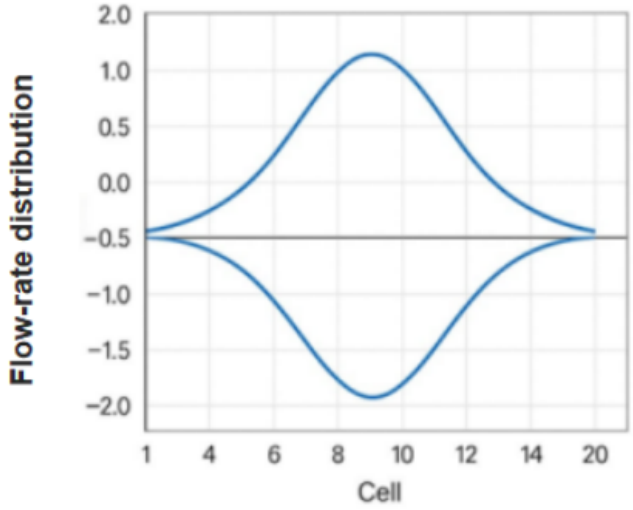


**Figure 4.** Modeled electrolyte flow-rate deviation profile showing symmetric non-uniformity across the 20-cell VRFB stack.

**Figure 4** illustrates the modeled electrolyte flow-rate distribution across the 20-cell VRFB stack, revealing a distinctly symmetric maldistribution pattern driven by manifold-induced pressure gradients. The terminal cells experience the highest relative flow rates (+1.92%), while the central cells receive the lowest (−1.11%), reflecting the inherent hydraulic resistance profile of the parallel flow network. This non-uniformity directly influences convective species transport, leading to localized concentration polarization and reduced electrochemical utilization in under-fed central cells. The figure highlights the critical role of optimized manifold and channel geometries in achieving uniform flow delivery and enhancing overall stack efficiency. Flow deviation peaked at the terminal cells (Cells 1 & 20: +1.92%) and was lowest at the central cells (Cells 10 & 11: −1.11%), a direct result of the pressure drops governed by the Darcy-Weisbach and Darcy's law formulations within the parallel flow circuit.

**Link to charge/discharge efficiency:** This flow maldistribution induces performance heterogeneity. Cells with lower flow rates suffer from inadequate convective species replenishment, elevating local concentration polarization and reducing efficiency. Optimizing manifold and channel geometries to homogenize this flow profile is a direct strategy for improving overall stack energy efficiency and accessible capacity.

### 3.3. Current variation and distribution in the stack

Analysis via the equivalent circuit model quantified substantial parasitic shunt currents within the manifold and channel network (**Figure 5**):

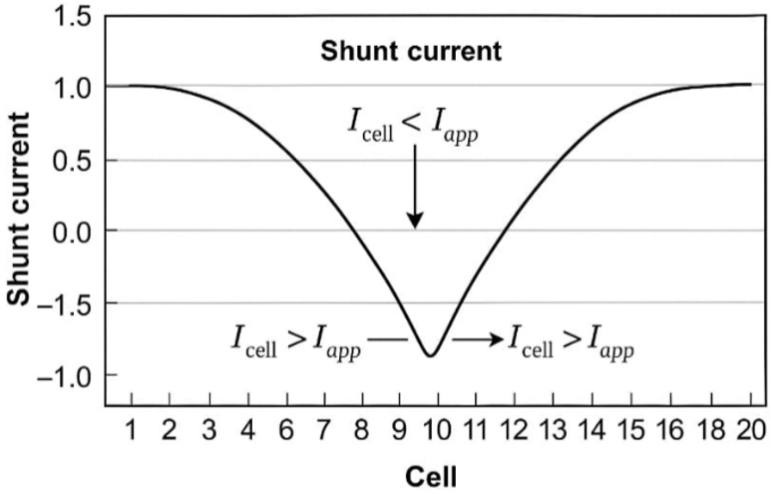


**Figure 5.** Modeled shunt-current variation along the VRFB stack, highlighting current reversal at the midpoint.

**Figure 5** presents the modeled distribution of parasitic shunt currents across the 20-cell VRFB stack, highlighting their characteristic symmetric behavior and direction reversal at the stack midpoint. The highest-magnitude shunt currents occur in the terminal cells, where the potential gradients between adjacent cells are strongest, while the minimum values appear at the central cells. This redistribution distorts the effective cell current: during charging, underfed cells experience a reduction in the available current for electrochemical reactions, with the effective cell current ($I_{\text{cell}}$) being lower than the applied current ($I_{\text{app}}$) in the central cells due to the diversion of current through shunt pathways; during discharging, the opposite trend emerges, with the effective cell current exceeding the applied current in the central cells as shunt currents augment the local current. The figure underscores the energetic and thermal penalties imposed by shunt pathways, which reduce round-trip efficiency and contribute to localized heating, thereby motivating manifold and channel design strategies aimed at minimizing these parasitic currents. These currents, driven by the potential gradient across series-connected cells, change direction at the stack's midpoint. Consequently, during charging, the effective cell current ($I_{\text{cell}}$) is lower than the applied current ($I_{\text{app}}$), and during discharging, it is higher.

**Link to performance enhancement & system compaction:** Shunt currents represent a direct energy loss, generating waste heat and accelerating uneven cell aging. Designing manifold geometry to minimize these parasitic currents directly improves round-trip efficiency. Furthermore, reducing this ancillary heat source simplifies thermal management needs, supporting system compaction by enabling smaller, more focused cooling solutions.

## 3.4. Voltage variation and distribution in the stack

The model predicts a symmetrical cell voltage distribution at the end of charge and discharge cycles, correlating with the flow and current profiles (**Figure 6**):

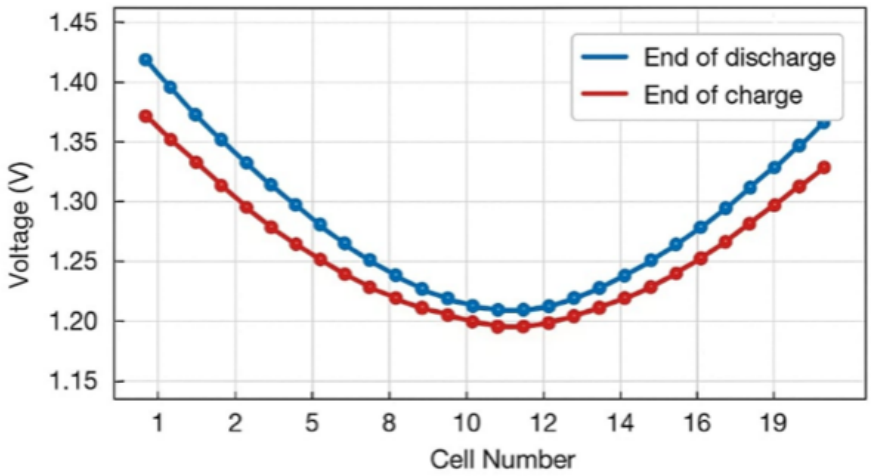


**Figure 6.** Modeled voltage distribution along the 20-cell VRFB stack at the end of charge and discharge cycles.

**Figure 6** illustrates the predicted symmetric voltage distribution across the 20-cell VRFB stack at the end of charge and discharge cycles. Terminal cells exhibit the highest voltages due to more favorable local current conditions and enhanced species availability, whereas the central cells show the lowest voltages, reflecting the combined effects of reduced flow rates and shunt-current redistribution. This characteristic voltage curvature highlights the inherent non-uniform electrochemical environment within the stack, where central cells reach cutoff limits earlier and thus constrain the overall accessible capacity. The figure underscores the necessity of harmonizing hydraulic and electrical design to reduce cell-to-cell voltage disparities and improve stack-level efficiency. Terminal cells exhibit higher voltages due to more favorable local currents (from shunt effects) and better species supply (from higher flow). Central cells show the lowest voltages, indicating constrained performance.

**Link to charge/discharge efficiency:** This voltage spread signifies unbalanced cell utilization. Central cells, limited by lower flow and influenced by shunt currents, reach cut-off voltages prematurely, thereby constraining the entire stack's energy throughput. Equalizing cell performance through hydraulic and electrical design optimization is therefore critical for maximizing overall efficiency.

## 3.5. Temperature variation and distribution

The coupled thermal energy balance ODEs accurately predict the stack's transient and steady-state thermal behavior. Key findings include: (1) The central cell (Cell 10) reaches the highest temperature, defining it as the critical point for thermal control. (2) The system attains a dynamic thermal equilibrium after several cycles. (3) Crucially, over 85% of the system's convective heat rejection occurs via the storage tanks, not the stack or pipes (**Figure 7)**.

The pie chart quantifies the percentage of total convective heat rejection attributed to the electrolyte storage tanks (85.8%), the stack assembly, and the connecting pipes, demonstrating the tanks' role as the primary thermal sink.

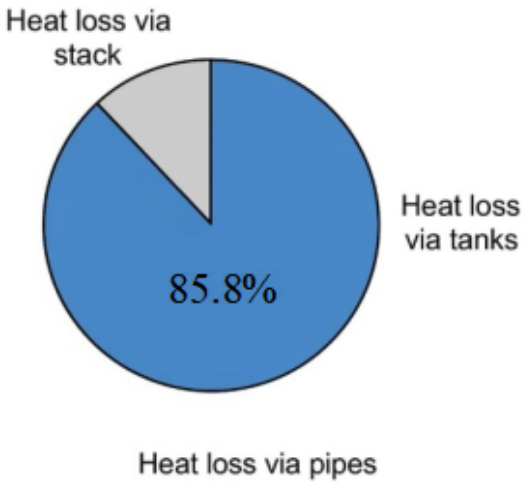


**Figure 7.** Distribution of convective heat loss across major VRFB system components.

**Figure 7** illustrates the distribution of convective heat loss across the major components of the VRFB system, revealing that the electrolyte storage tanks dominate the thermal rejection pathway, accounting for approximately 85.8% of total heat dissipation. In contrast, the stack and connecting pipes contribute only marginally to overall thermal losses. This pronounced imbalance highlights the tanks as the primary thermal bottleneck, providing a compelling basis for shifting from conventional room-level cooling to a targeted, tank-focused thermal management strategy.

**Primary link to system compaction:** This finding is transformative for thermal management design. It demonstrates that maintaining stack temperature below the critical 40 °C threshold does not require cooling the entire enclosure. A novel tank-focused cooling strategy is validated, which reduces the volume requiring active temperature control by ~60% and lowers associated cooling energy consumption by 27.18% compared to conventional room-cooling methods. This insight enables a radical redesign for more compact, cost-effective, and energy-efficient VRFB systems by relocating the primary thermal management interface from the stack to the storage tanks.

## 4. VRFB cooling control strategy: Model-based optimization for efficiency and compaction

The validated multi-physics model identifies thermal management as a critical lever for performance enhancement and system integration. To prevent performance decay and safety risks from vanadium precipitation (>40 °C), an active cooling strategy is essential. This section employs the model to design, evaluate, and time cooling strategies, directly linking system dynamics to tangible gains in energy efficiency and hardware simplification for system compaction.

### 4.1. Room gas flow cooling control model

A dynamic thermal model for a climate-controlled room housing the VRFB system was developed using energy balance ODEs. This model calculates the air conditioning (AC) power requirement ($P_{ac}$) by accounting for three principal loads: the energy to

initially cool the room air ($P_{\text{in}}$), continuous heat loss through the walls to the external environment ($P_{\text{loss}}$), and the heat rejected from the VRFB system into the room ($P_{\text{heat}}$). The governing equations are:

$$P_{\text{in}} = M_{air} C_{air} (T_{\text{air}} - T_{\text{room}}) \tag{24}$$

$$P_{\text{loss}} = \int U_{\text{wall}} A_{\text{wall}} (T_{\text{air}} - T_{\text{room}}) dt \tag{25}$$

$$P_{\text{heat}} = \int q_{\text{heat}} dt \tag{26}$$

$$P_{ac} = \frac{P_{\text{in}} + P_{\text{heat}} + P_{\text{loss}}}{\text{EER}} \tag{27}$$

Here, $M_{air}$ and $C_{air}$ are the mass and heat capacity of the room air, $A_{\text{wall}}$ and $U_{\text{wall}}$ are the wall's heat transfer coefficient and area, $T_{\text{air}}$ and $T_{\text{room}}$ are the ambient and room temperatures, and EER is the Air Conditioning's Energy Efficiency Ratio. The heat load from the VRFB, $q_{\text{heat}}$, is calculated by the stack model and differs between strategies. This control-theoretic model enables the quantitative comparison of cooling energy consumption for different approaches.

## 4.2. Common room cooling control strategy

The conventional approach places the entire VRFB system (stack, pipes, tanks) in a single, large climate-controlled room. The model was used to determine the precise control parameters needed at an ambient temperature of 30 °C. To reliably maintain the critical central cell below 40 °C, the strategy must initiate cooling preemptively when the stack reaches 38.5 °C and maintain a room temperature of 26.7 °C (**Figure 8**):

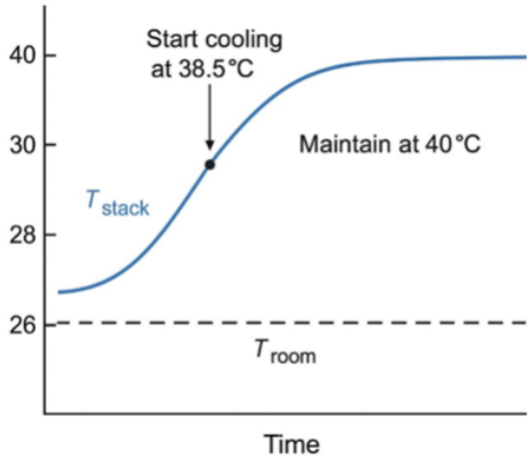


**Figure 8.** Temperature control profile for the common room cooling strategy.

**Figure 8** illustrates the thermal response of the VRFB stack under the conventional room cooling strategy. Cooling is activated preemptively when the stack temperature reaches 38.5 °C, after which the ambient room temperature is maintained at 26.7 °C. The stack temperature subsequently approaches a steady-state value near 40 °C, indicating that the system remains within the safe operational window but at the cost of cooling

a large, thermally inefficient volume. The figure highlights the inherent limitations of room-based cooling, where substantial energy is expended to regulate components that contribute minimally to the system's total heat rejection. This approach ensures safe operation but is inherently inefficient, as it consumes energy to cool all system components, including the stack and pipes, which contribute minimally to the overall heat rejection footprint.

### 4.3. New tank cooling control strategy

Informed by the model's key finding that over 85% of convective heat loss occurs at the tanks (Section 3.5), an innovative targeted cooling strategy was developed. This strategy proposes isolating only the electrolyte storage tanks in a small, cooled enclosure, while the stack resides in a separate, ventilated space at ambient temperature.

Performance Enhancement & System Compaction: This paradigm shift delivers direct, quantifiable benefits:

**Dramatic energy savings:** By cooling only the primary thermal mass (the tanks), the required control volume and thermal load are drastically reduced. The model demonstrates that this strategy achieves the same thermal safety ($T_{stack} < 40$ °C) while reducing cooling energy consumption by 27.18% over 20 cycles compared to the common room strategy (**Figure 9**):

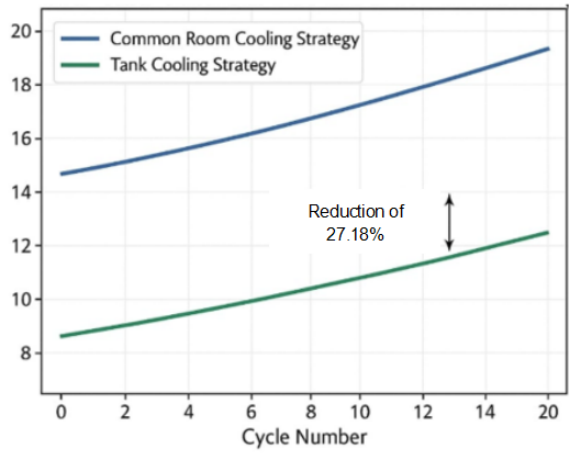


**Figure 9.** Comparison of cooling energy consumption between common room cooling and tank cooling strategies across 20 cycles.

**Figure 9** compares the auxiliary cooling energy required for two distinct thermal management strategies across 20 complete charge-discharge cycles. The conventional method, which involves cooling the entire system room, displays consistently high and stable energy demand, a direct consequence of the thermodynamic inefficiency in conditioning a large, static air volume. Conversely, the proposed tank-focused strategy exhibits a markedly lower and dynamically responsive energy profile. Quantitative analysis reveals that by the final cycle, this targeted approach achieves a cumulative reduction in cooling energy consumption of 27.2%. The data clearly demonstrates that concentrating thermal regulation on the electrolyte, the system's primary thermal mass within the storage tanks, yields substantial efficiency improvements over conditioning the entire enclosure. The implementation of this strategy delivers three principal

system-level advancements:

**Facilitated system compaction:** By localizing cooling to the tanks, the design of the stack enclosure is liberated from the requirements of integrated, bulky cooling infrastructure. The need for complex air sealing, dedicated ductwork, and forced-air circulation around the stack is eliminated. This enables a significantly more compact and mechanically simplified stack design, reducing overall system footprint.

**Enhanced net system efficiency:** The drastic reduction in the auxiliary power load for cooling directly contributes to a higher net round-trip energy efficiency for the entire VRFB system, improving its economic metrics.

**Model-informed optimal control:** The strategy's efficacy validates a control co-design paradigm. Critical operational parameters, including the optimal cooling activation temperature of 38.5 °C and the tank room setpoint of 26.3 °C, were identified through simulation, demonstrating how the mathematical model directly generates efficient control logic to realize performance gains.

In summary, the shift from whole-room to tank-focused cooling exemplifies how a fundamental multi-physics model evolves from an analytical diagnostic into a transformative design instrument. It provides a direct pathway to realizing a more energy-efficient and physically compact system architecture, directly addressing key economic and integration barriers that have historically impeded the widespread deployment of vanadium redox flow batteries.

## 5. Conclusions

This research introduces a validated, system-level modeling framework that unifies the interdependent physics governing vanadium redox flow battery (VRFB) stack operation. The model simultaneously resolves electrolyte flow, mass and charge transport, electrochemical kinetics, parasitic shunt currents, and their collective thermal effects, providing a holistic view of stack behavior. A key outcome of this integration is the quantification of inherent spatial gradients, revealing significant cell-to-cell variations in flow, current density, and temperature that critically impact overall performance and durability. Analysis identifies a pronounced thermal challenge: under high-current operation, cells in the central region of the 20-cell stack consistently evolve into hotspots, surpassing the 40 °C threshold critical for preventing vanadium precipitation and associated performance degradation. To mitigate this risk without incurring excessive energy penalties, an innovative, system-aware cooling strategy is developed. This method shifts the focus of thermal management from the entire stack enclosure to a targeted regulation of the electrolyte within the external storage tanks. By precooling the inlet electrolyte, this tank-focused strategy successfully maintains all cells below the critical temperature limit. System-level simulations demonstrate that this approach achieves a 27.2% reduction in the auxiliary energy required for cooling across extended cycling, compared to conventional full-room climate control. This results in a more sustainable and cost-effective thermal management paradigm. This paradigm not only resolves an immediate thermal challenge but also establishes a modular framework amenable to future enhancements in scale, intelligence, and longevity. The study underscores that a coupled multi-physics

perspective is essential for bridging the gap between fundamental electrochemistry and practical system engineering. Looking forward, the integration of Physics-Informed Neural Networks (PINNs) with the established multi-physics framework presents a promising avenue to evolve the model into an adaptive digital twin. Such a hybrid system would enhance real-time predictive control, enable autonomous optimization of flow and cooling setpoints, and further reduce uncertainty in long-duration performance forecasting—key steps toward commercially resilient, grid-integrated VRFB systems. The findings provide both a deeper mechanistic understanding of internal transport limitations and a directly applicable design strategy for efficient, reliable VRFB systems. Looking ahead, this unified multi-physics framework opens several compelling research frontiers:

(1) Scaling and System Integration—Investigating how the targeted tank-cooling strategy and flow-distribution insights scale to megawatt-class stacks with hundreds of cells, where manifold architecture and control dynamics become critically complex.
(2) Intelligent Digital Twins via Hybrid Modeling—Integrating Physics-Informed Neural Networks (PINNs) to transform the model into a real-time capable digital twin, enabling adaptive control, fast inverse design, and uncertainty quantification for operational resilience.
(3) Lifetime and Degradation Integration—Extending the framework to incorporate long-term electrolyte aging, membrane degradation, and precipitation kinetics, thereby enabling health-aware operation and total-cost-of-ownership optimization.

These directions will further bridge high-fidelity physics with smart system operation, accelerating the development of economically competitive grid-scale storage solutions.

**Author contributions:** Conceptualization, JH and LA; validation, JH, LA, and CH; formal analysis, JH and CH; investigation, JH, LA, and CH; resources, JH and LA; data curation, CH and AK; writing—original draft preparation, JH, LA, and MB; writing—review and editing, JH, AK, and MB; visualization, JH and MB; supervision, JH, AK, and MB; project administration, AK and MB; funding acquisition, LA. All authors have read and agreed to the published version of the manuscript.

**Funding:** This research was funded by the Deanship of Scientific Research of Taif University, grant number 83/Deanship-of-Scientific-Research and the APC was funded by the Deanship of Scientific Research of Taif University (DSRTU) (https://www.tu.edu.sa/En/Deanships/110/Deanship-of-Graduate-Studies-and-Scientific-Research).

**Institutional review board statement:** Not applicable. Based on the content of the manuscript, which is a modeling and simulation study involving a theoretical framework for vanadium redox flow batteries (VRFBs), the research does not involve human participants, animal subjects, or any primary data collection from living beings. The study is purely computational and analytical, based on established physics and validated against literature data.

**Informed consent statement:** Not applicable. Based on the manuscript content, this

is a computational modeling study and does not involve human participants or patient data.

**Data availability statement:** The data used in this study are available from the corresponding author upon reasonable request.

**Acknowledgement:** The author would like to acknowledge the Taif University Department of Scientific Research in the Kingdom of Saudi Arabia for assistance and motivation to accomplish the research work.

**Conflict of interest:** The authors declare no conflict of interest to report regarding the present study.

## References

1. Agyekum EB, Abdullah M, Odoi-Yorke F, et al. A state-of-the-art review of electrolyte systems for vanadium redox flow battery—Status of the technology, and future research. Energy Conversion and Management: X. 2025; 27: 101180. doi: 10.1016/j.ecmx.2025.101180
2. Shahid H, Uddin E, Abdelkefi A, et al. Effectiveness of energy harvesting systems subjected to flow-induced vibrations in confined spaces. Renewable and Sustainable Energy Reviews. 2025; 210: 115183. doi: 10.1016/j.rser.2024.115183
3. Ren J, Wei L, Wang Z, et al. An electrochemical-thermal coupled model for aqueous redox flow batteries. International Journal of Heat and Mass Transfer. 2022; 192: 122926
4. Xiong B, Ding Y, Zhang Q, et al. Finite element-based analysis of composite serpentine flow channel 3D modeling of vanadium redox flow battery. International Journal of Green Energy. 2025; 22(5): 831–838. doi: 10.1080/15435075.2021.2007390
5. He K, Banerjee A. Dynamic behavior and energy harvesting potential of a circular cylinder experiencing flow-induced motions in elevated turbulent inflow. Renewable Energy. 2026; 261: 125231. doi: 10.1016/j.renene.2026.125231
6. Yu Y, Hu G, Liu C, et al. Prediction of solar irradiance one hour ahead based on quantum long short-term memory network. IEEE Transactions on Quantum Engineering. 2023; 4: 1–15. doi: 10.1109/TQE.2023.3271362
7. Chu F, Xiao G, Xia L, et al. Analysis of battery performance and mass transfer behavior for organic redox flow battery with different flow fields. Journal of The Electrochemical Society. 2022; 169: 070529. doi: 10.1149/1945-7111/ac81f4
8. Zheng Y, Qu D, Yang, F, et al. Study on performance improvement of vanadium redox flow batteries focused on electrode fabrication parameters and compression strategies. Journal of Energy Storage. 2025; 109: 115142. doi: 10.1016/j.est.2024.115142
9. Komuro Y, Uchimichi N, Kondo Y, et al. Development of gas-liquid interfacial velocity correlation for flow-induced vibration analysis of triangular array tube bundle in steam generators. Progress in Nuclear Energy. 2026; 191: 106099. doi: 10.1016/j.pnucene.2025.106099
10. Tong Z, Shu Z, Liu D, et al. Investigating flow-induced vibration in pump-turbines using a multi-scale fluid-structure interaction approach considering clearance flow effects. Sustainable Energy Technologies and Assessments. 2025; 82: 104487. doi: 10.1016/j.seta.2025.104487
11. Liu Y, He Y. Recent Advances in Numerical Modeling of Aqueous Redox Flow Batteries. Energies. 2025; 18(15): 4170. doi: 10.3390/en18154170
12. Merzari E, Brockmeyer L, Yuan H, et al. Chapter 29—Helical-coil steam generators: Application of computational fluid–structure interaction/flow-induced vibration for heat exchangers and steam generators. In: Riznic J (editor). Steam Generators for Nuclear Power Plants, 2nd ed. Woodhead Publishing; 2026. pp: 673–705.
13. Weber AZ, Mench MM, Meyers J, et al. Redox flow batteries: A review. Journal of Applied Electrochemistry. 2011; 41(10): 1137–1164. doi: 10.1007/s10800-011-0348-3
14. Legros B, Thivel PX, Bultel Y, et al. First results on PEMFC diagnosis by electrochemical noise. Electrochemistry Communications. 2011; 13(12): 1514–1516. doi: 10.1016/j.elecom.2011.10.007
15. Cordero Obando A, Hourigan K, Thompson MC, et al. Flow-induced vibration of an elastically mounted oblate spheroid with variable mass ratio. International Journal of Heat and Fluid Flow. 2026; 117(Part B): 110129. doi: 10.1016/j.ijheatfluidflow.2025.110129

16. Zheng Y, Shi P, Sun Z, et al. Hybrid EXP-FEA-ANN modeling for citrus ripeness detection via modal analysis. Journal of Stored Products Research. 2026; 115: 102801. doi: 10.1016/j.jspr.2025.102801
17. Xiong J, Dong X, Song Y, et al. A high performance Ru–$ZrO_2$/carbon nanotubes–Ni foam composite catalyst for selective CO methanation. Journal of Power Sources. 2013; 242: 132–136. doi: 10.1016/j.jpowsour.2013.05.084
18. Liu X, Pan L, Rao H, et al. A review of transport properties of electrolytes in redox flow batteries. Future Batteries. 2025; 5: 100019. doi: 10.1016/j.fub.2024.100019
19. Suba M, Vallayil P, Jaiswal N, et al. Advances in redox flow batteries—A comprehensive review on inorganic and organic electrolytes and engineering perspectives. Advanced Energy Materials. 2024; 14(32): 2400721. doi: 10.1002/aenm.202400721
20. Lewis SD, Chippar P. Analysis of heat and mass transfer during charging and discharging in a metal hydride–phase change material reactor. Journal of Energy Storage. 2021; 33: 102108. doi: 10.1016/j.est.2020.102108
21. Tang A, McCann J, Bao J, et al. Investigation of the effect of shunt current on battery efficiency and stack temperature in vanadium redox flow battery. Journal of Power Sources. 2013; 242: 349–356.
22. Yang L, Li S, Hou J. A comprehensive review of flow-induced vibration and fatigue failure in the moving components of control valves. Machines. 2025; 13(9): 766. doi: 10.3390/machines13090766
23. Zheng H, Li M, Wang J, et al. A numerical study on flow-induced vibration of a buoy-mooring system. Marine Structures. 2026; 106: 103975. doi: 10.1016/j.marstruc.2025.103975
24. Clemente León A. Vanadium Redox Flow Battery Modeling. In: Modeling and Control of a Vanadium Redox Flow Battery. Springer Theses. Springer; 2025. doi: 10.1007/978-3-031-80728-2_4
25. Shah AA, Watt-Smith MJ, Walsh FC. A dynamic performance model for redox-flow batteries involving soluble species. Electrochimica Acta. 2008; 53(27): 8087–8100. doi: 10.1016/j.electacta.2008.05.067
26. Chen Z, Zhang Z, Xu Y, et al. Aerodynamic characteristics and flow field characteristics of rigid and forced-vibration square cylinders in turbulent flow. Physics of Fluids. 2026; 38: 015124. doi: 10.1063/5.0305104
27. Skyllas-Kazacos M, McCann J, Li Y, et al. The mechanism and modelling of shunt current in the vanadium redox flow battery. ChemistrySelect. 2016; 1(10): 2249–2256. doi: 10.1002/slct.201600432
28. Pu H, Liu L, Chang Z, et al. Organic/inorganic composite membranes based on polybenzimidazole and nano-$SiO_2$. Electrochimica Acta. 2009; 54(28): 7536–7541. doi: 10.1016/j.electacta.2009.08.011